



Technical Note

Satellite Retrieval of Air Pollution Changes in Central and Eastern China during COVID-19 Lockdown Based on a Machine Learning Model

Zigeng Song^{1,2}, Yan Bai^{2,3}, Difeng Wang^{2,3}, Teng Li² and Xianqiang He^{2,4,*}¹ College of Oceanography, Hohai University, Nanjing 210098, China; 190811080001@hhu.edu.cn² State Key Laboratory of Satellite Ocean Environment Dynamics, Second Institute of Oceanography, Ministry of Natural Resources, Hangzhou 310012, China; baiyan@sio.org.cn (Y.B.); dfwang@sio.org.cn (D.W.); litengh@126.com (T.L.)³ Southern Marine Science and Engineering Guangdong Laboratory (Guangzhou), Guangzhou 510000, China⁴ School of Oceanography, Shanghai Jiao Tong University, Shanghai 200030, China

* Correspondence: hexianqiang@sio.org.cn

Abstract: With the implementation of the 2018–2020 Clean Air Action Plan (CAAP) the and impact from COVID-19 lockdowns in 2020, air pollution emissions in central and eastern China have decreased markedly. Here, by combining satellite remote sensing, re-analysis, and ground-based observational data, we established a machine learning (ML) model to analyze annual and seasonal changes in primary air pollutants in 2020 compared to 2018 and 2019 over central and eastern China. The root mean squared errors (RMSE) for the PM_{2.5}, PM₁₀, O₃, and CO validation dataset were 9.027 µg/m³, 20.312 µg/m³, 10.436 µg/m³, and 0.097 mg/m³, respectively. The geographical random forest (RF) model demonstrated good performance for four main air pollutants. Notably, PM_{2.5}, PM₁₀, and CO decreased by 44.1%, 43.2%, and 35.9% in February 2020, which was likely influenced by the COVID-19 lockdown and primarily lasted until May 2020. Furthermore, PM_{2.5}, PM₁₀, O₃, and CO decreased by 16.4%, 24.2%, 2.7%, and 19.8% in 2020 relative to the average values in 2018 and 2019. Moreover, the reduction in O₃ emissions was not universal, with a significant increase (~20–40%) observed in uncontaminated areas.

Keywords: air pollutants concentration; COVID-19 lockdown; machine learning; satellite remote sensing

Citation: Song, Z.; Bai, Y.; Wang, D.; Li, T.; He, X. Satellite Retrieval of Air Pollution Changes in Central and Eastern China during COVID-19 Lockdown Based on a Machine Learning Model. *Remote Sens.* **2021**, *13*, 2525. <https://doi.org/10.3390/rs13132525>

Academic Editor: Costas Varotsos

Received: 31 May 2021

Accepted: 24 June 2021

Published: 28 June 2021

Publisher's Note: MDPI stays neutral with regard to jurisdictional claims in published maps and institutional affiliations.



Copyright: © 2021 by the authors. Licensee MDPI, Basel, Switzerland. This article is an open access article distributed under the terms and conditions of the Creative Commons Attribution (CC BY) license (<https://creativecommons.org/licenses/by/4.0/>).

1. Introduction

With the rapid economic growth, industrialization, and urbanization of China, particulate matter (PM), including PM₁₀ and PM_{2.5} (<10- and <2.5-micron diameters, respectively), and gaseous pollutants, such as sulfur dioxide (SO₂), ozone (O₃), carbon monoxide (CO), and nitrogen oxides (NO_x), have become a serious concern. In 2012, to improve ambient air quality, the Chinese government issued stringent national ambient air quality standards (NAAQS) [1] and enhanced the monitoring of six major air contaminants (PM₁₀, PM_{2.5}, SO₂, NO₂, CO, and O₃) in 338 Chinese cities [2], with mixed results. For example, the Atmospheric Pollution Prevention and Control Action Plan (2013–2017) greatly contributed to the reduction in PM_{2.5} [3,4]. However, although various studies have reported an improvement in ambient air quality, O₃ concentrations have shown an increasing trend in the last five years [4–6].

The implementation of the second-phase Clean Air Action Plan (CAAP) has been impacted by the coronavirus disease 2019 (COVID-19) outbreak during the Chinese New Year holiday (24 January to 8 February 2020) [7,8]. The Chinese government implemented strict lockdown measures during (and beyond) the festival period. Efforts to contain the rapid spread of COVID-19 drastically reduced human activities worldwide, including industrial production, energy consumption, and transportation. Of note, air pollutant emissions also rapidly decreased during the lockdown period [9–12]. Liu et al., reported

a 77% decrease in NO_x , leading to a significant increase of O_3 in Hangzhou during the COVID-19 lockdown [13]. Bao et al., found that $\text{PM}_{2.5}$, PM_{10} , and CO decreased by 5.93%, 13.66%, and 4.58%, respectively, in 44 cities of northern China [14]. Thus far, however, most studies have assessed changes in primary air pollutants before April 2020, without considering temporal environmental hysteresis [15–19].

Of interest, several studies have reported that despite the decrease in air pollutant emissions in January and February 2020, severe haze episodes in northern China did not show an associated improvement [12,15,20]. These anomalous changes have caused public controversy about the actual effects of the CAAP [8]. However, short-term responses in air quality to variations in anthropogenic emissions may not be obvious at the regional meteorological scale [21]. For example, Li et al., reported that environmental regulations have a stronger hysteresis impact on air pollutants in eastern China than in western China [17]. In addition, the influence of transboundary air pollutants can also lead to uncertainties in assessing the impacts of exhaust emission control on air pollutant reduction over short periods in small regions [21,22]. Therefore, short-term investigations on the changes in air pollutants during the first few months of 2020, as opposed to examining annual variations, are insufficient.

As for the long-term prediction in the geosciences, machine learning (ML) algorithms have demonstrated that they deal with non-linear processes well [23]. Several studies have successfully applied ML algorithms to estimate $\text{PM}_{2.5}$ and PM_{10} concentrations in China based on satellite remote sensing and meteorological data. Liu et al., developed a ML model to predict the surface O_3 in China from 2005 to 2017 and obtained the results with high accuracy [24]. These studies have produced most air pollutants data with high quality and spatial coverage, but still lack CO and other air pollutant predictions [24–26]. Moreover, the comprehensive assessments of spatiotemporal distributions of air pollutants and their changes are still deficient during COVID-19 lockdown [14]. Therefore, in the current study, we utilized the ML approach to determine the concentrations of $\text{PM}_{2.5}$, PM_{10} , O_3 , and CO in central and eastern China. We further analyzed the spatiotemporal distributions and changes in these primary air pollutants from 2018 to 2020 and explored the impact of COVID-19 lockdown on ambient pollution.

2. Materials and Methods

2.1. Study Area

The study area and air quality monitoring stations in 22 provinces and municipalities of central and eastern mainland China are shown in Figure 1a and include economically developed megacities within the Beijing-Tianjin-Hebei Region (BTH), Yangtze River Delta (YRD), and Guangdong-Hong Kong-Macao Greater Bay Area (GBA). These stations and ground-based observations provide a broad range of air monitoring capabilities and data for these regions. Furthermore, the population in the 22 provinces accounts for 82.4% of the total population in China, and Gross Domestic Product (GDP) accounts for 86.2% of the national total according to the China Statistical Yearbook (2019) [27]. Since 2013, the Chinese government has implemented various stringent pollution control policies, resulting in a significant improvement in ambient air quality. COVID-19 lockdowns in early 2020 further enhanced these reductions in emissions. The joint effects of the CAAP and COVID-19 lockdowns have reduced human activities and improved the air environment. Therefore, understanding the concentrations of and changes in air pollutants from 2018 to 2020 is of great significance for future environmental protection and public health in central and eastern China.

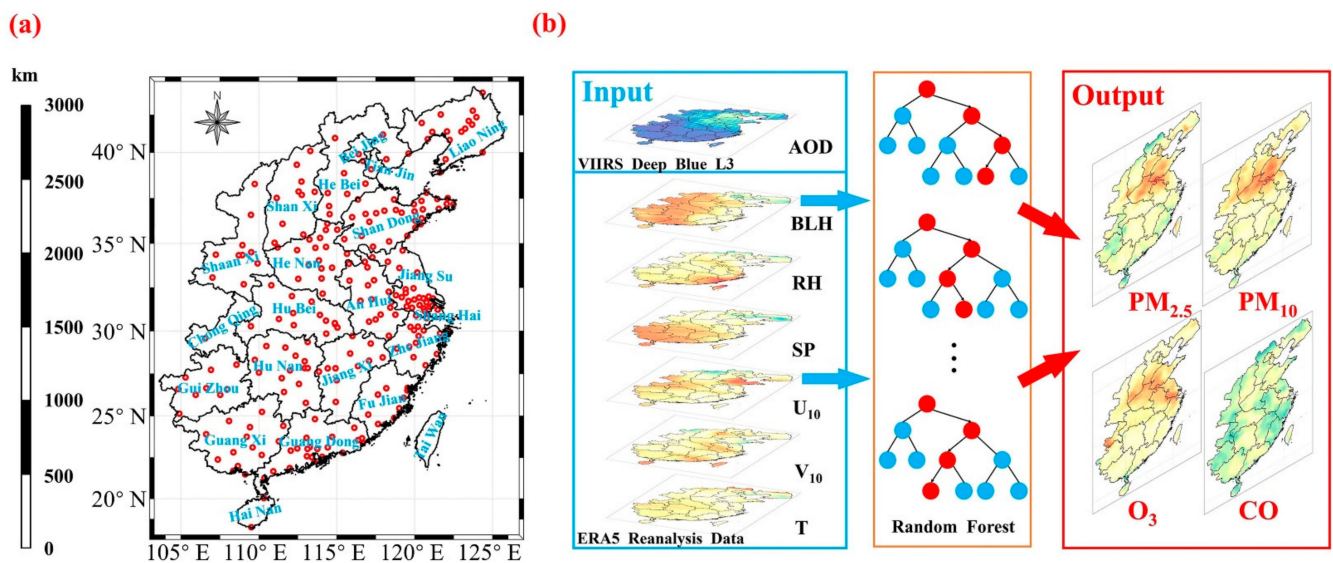


Figure 1. (a) Study area, including 22 provinces and air quality monitoring stations (red dots) in the central and eastern China; (b) Schematics of geographical random forest (RF) model.

2.2. Data Description

The ground-based observational data of the four air pollutants (PM_{2.5}, PM₁₀, O₃, and CO) used in this research were provided by the China National Environmental Monitoring Center (CNEMC, see <http://www.cnemc.cn/en/>, accessed on 10 May 2021). The CNEMC provides hourly, 8 h, and 24 h moving average concentrations for air quality index (AQI), PM_{2.5}, PM₁₀, O₃, SO₂, NO₂, and CO for each station or city. Detailed measurement and quality control (QC) descriptions are available from the China Ministry of Ecology and Environment (MEE, see <http://www.mee.gov.cn/>, accessed on 10 May 2021).

The Suomi National Polar-Orbiting Partnership (Suomi NPP) spacecraft, which launched on 28 October 2011, carries the Visible Infrared Imaging Radiometer Suite (VIIRS), with 22 radiometric bands ranging from 0.41 to 12.5 microns and a 3060 km swath. We used the VIIRS Level 3 daily deep blue aerosol products (AERDB_D3_VIIRS_SNPP, see <https://ladsweb.modaps.eosdis.nasa.gov/search/>, accessed on 10 May 2021) from 2018 to 2020, which are derived from VIIRS Level 2, 6 min and swath-based aerosol products gridded on a 1° by 1° horizontal resolution grid. The use of aggregated products can improve data validity and avoid outliers.

We used the European Centre for Medium-Range Weather Forecasts (ECMWF) 5th Re-Analysis (ERA5, see <https://cds.climate.copernicus.eu/#!/home>, accessed on 10 May 2021) dataset with 0.25° grid resolution from 2018 to 2020. According to previous study and correlation analysis (Figure 2), we selected hourly meteorological data from the ERA5 re-analysis dataset, which included relative humidity (RH, %), surface pressure (SP, Pa), air temperature (T, K), boundary layer height (BLH, m), u-component of wind above 10 m (U₁₀, m/s), and v-component of wind above 10 m (V₁₀, m/s), with the hourly dataset then converted to a daily scale.

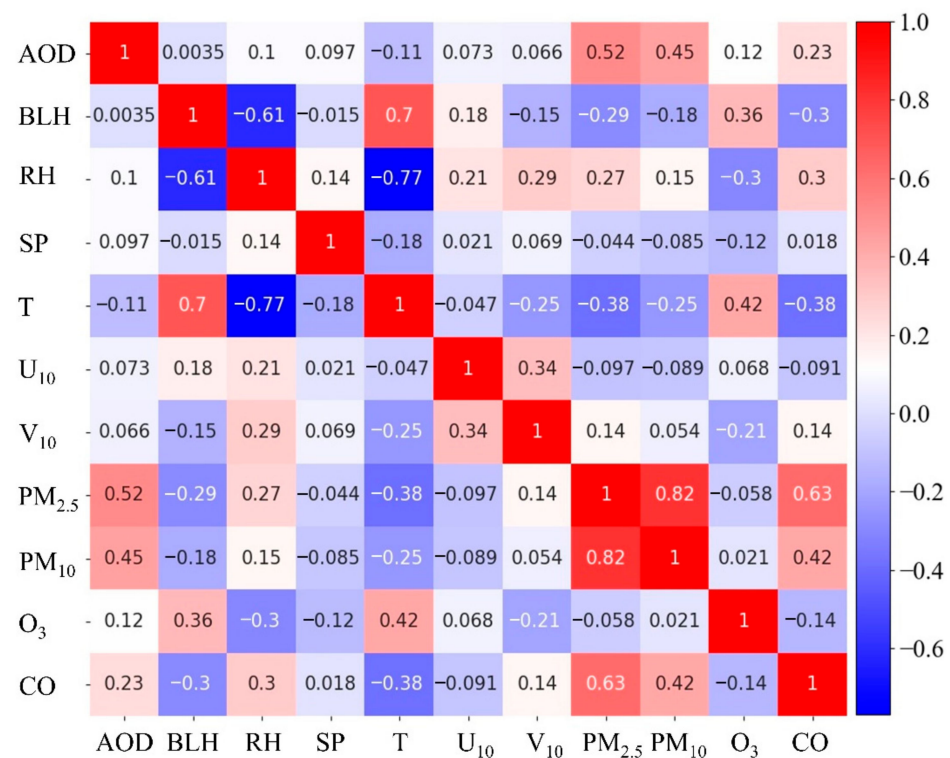


Figure 2. The correlative analysis between input and output variables.

2.3. ML Algorithm

In recent years, an ML algorithm has been widely applied in air pollutants prediction mainly due to the superior ability of ML algorithms to capture and employ the features of independent variables and solve complex non-linear problems [25,26,28,29]. Air pollutants are non-linearly affected by multiple ambient factors, such as T, RH, SP, and wind speed. As shown in Figure 2, meteorological factors significantly influenced the concentration of air pollutants (PM_{2.5}, PM₁₀, O₃, and CO) and showed relatively strong relationships with aerosol optical depth (AOD) and T. Conventional statistical models have difficulty in addressing the complex non-linear relationship among meteorological factors and air pollutant concentrations. Therefore, ML models can be utilized to resolve this non-linear problem [26].

The random forest (RF) model is a family of ML algorithms and constituted by an ensemble of decision trees. The RF regression model has relatively low generalization error based on ensemble decision tree theory and generates an unbiased output by aggregating the importance of each regression tree branch feature [30]. In the process of RF regression model simulations, the optimal splitting method can be used to split the samples for each regression tree according to the data characteristics, as shown in the red chain in Figure 1b. The detailed structures of RF algorithm for the PM_{2.5}, PM₁₀, O₃, and CO are presented in Figures S1–S4.

Considering the differences in resolution between AOD and meteorological data, we interpolated their resolutions linearly to a 0.5° grid for the model input. To assess the relationships among the concentrations of the four air pollutants and input variables, we co-matched ground-based observational data to the nearest input pixel. The specific structure and schematics of the geographical RF model are illustrated in Figure 1b. Following previous research, we set the forest to 2000 trees, maximum depth of trees to 15, and minimum number of splitting samples to 10 [25,31]. Input variable features were extracted by model training and their relative feature importance (RFI) was determined as a predictor. Additionally, sample-based 10-fold cross-validation (CV) was applied to optimize model

performance. The RF model emphasizes practical application for substantive interpretation by calculating variable importance compared to neural network (NN) models [30].

3. Results and Discussion

3.1. Evaluation of Model Performance

As shown in Figure 3, the coefficients of determination (R^2) between the RF-model predicted and ground-measured air pollutant concentrations were above 0.925 during training (2018–2019) and above 0.883 for independent validation (2020). The root mean squared errors (RMSE) for the $PM_{2.5}$, PM_{10} , O_3 , and CO validation dataset were $9.027 \mu\text{g}/\text{m}^3$, $20.312 \mu\text{g}/\text{m}^3$, $10.436 \mu\text{g}/\text{m}^3$, and $0.097 \text{mg}/\text{m}^3$, respectively. The R^2 and RMSE values of the validation dataset were weaker than those of the training dataset, but were within the permissible range. However, the model tended to underestimate air pollutant levels under high-concentration conditions, which is expected in most ML algorithms [32]. The robustness of the O_3 model was better than that of the other three air pollutant models due to its higher correlations with T, BLH, and RH (correlation coefficients (R) of 0.42, 0.36, and -0.3 , respectively) (Figure 3). The RFI of the predictors can be shown in Figure 4. We can find that the two most important predictors of $PM_{2.5}$ and PM_{10} are AOD and T, whereas the two most important predictors of O_3 and CO are T and BLH. The larger RFI means that the predictor contributes more on the output variable. Thus, in geographical RF models, AODs mainly regulate the changes of $PM_{2.5}$ and PM_{10} , while T mainly controls the changes of O_3 .

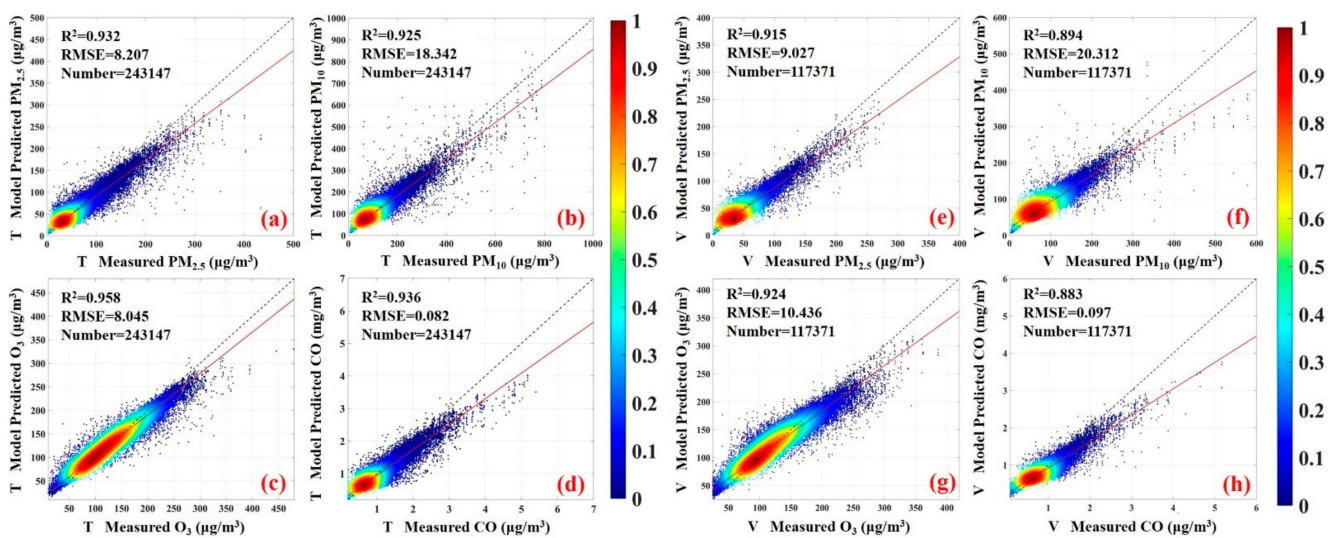


Figure 3. Density plots of daily $PM_{2.5}$, PM_{10} , O_3 , and CO concentrations for model training and independent validation. The results for (a–d) model training (2018–2019) and (e–h) independent validation (2020) for $PM_{2.5}$, PM_{10} , O_3 , and CO concentration.

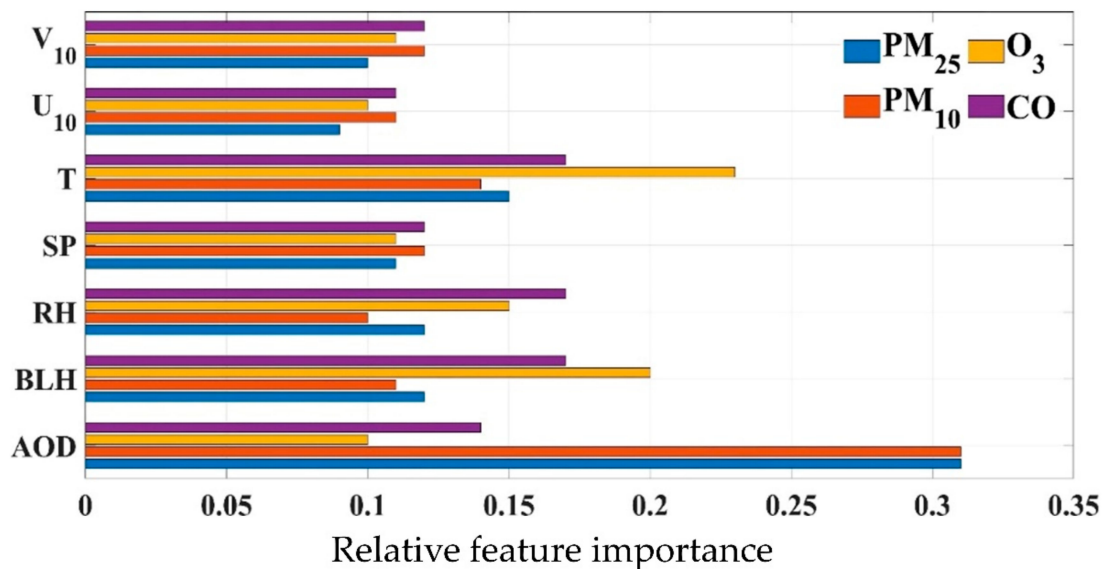


Figure 4. Relative feature importance of the predictors in geographical RF model simulations.

The performance of geographical RF models also need to be diagnosed by the learning curves, which are shown in Figure 5. The learning curve represents the changes in performance score for training and cross-validation with the sample size. Here, the performance score of geographical RF models are determined based on the sample-based 10-fold CV method. As Figure 5a–d show, the CV performance scores are enhanced with the increases of the training dataset size, suggesting that larger training dataset can further improve the model performance. Additionally, the impacts of training dataset size on the performance scores of PM_{2.5} and PM₁₀ are stronger than of O₃ and CO. Overall, our results indicated that four air pollutants concentrations could be accurately predicted using the geographical RF model.

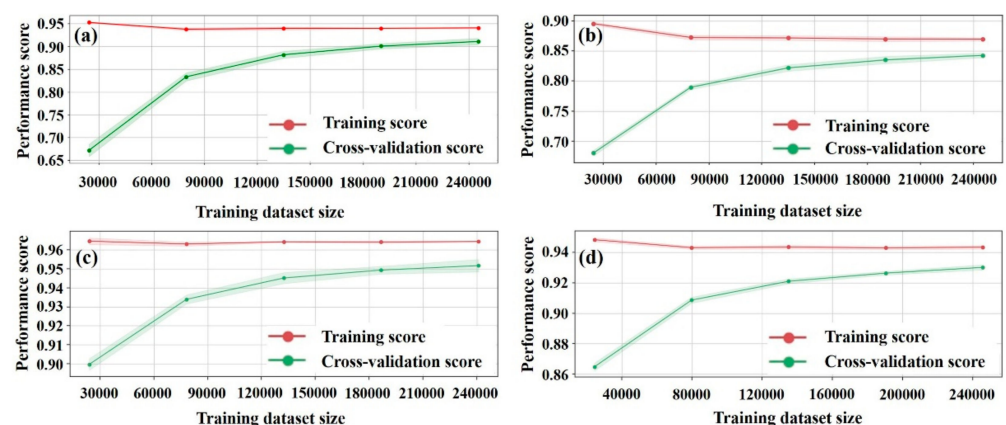


Figure 5. The learning curve of the geographical RF models for (a) PM_{2.5}, (b) PM₁₀, (c) O₃, and (d) CO.

3.2. Annual Changes in Air Pollutants in 2020 Compared to 2018 and 2019

Figure 6a depicts the spatial distribution and variation of the PM_{2.5}, PM₁₀, O₃, and CO concentrations in February, May, August, and November 2020 in central and eastern China. Figure 6b shows the annual average changes in four pollutants concentrations relative to their averages in 2018 and 2019. Under the joint impact of COVID-19 lockdown and the CAAP, the PM_{2.5}, PM₁₀, and CO concentrations declined, on average, by 16.4%, 24.2%, and 19.8%, respectively, in 2020. Almost all regions in central and eastern China showed

a decline in $PM_{2.5}$, PM_{10} , and CO, indicating that short-term control of production may improve the air environment quality over a relatively long-term period.

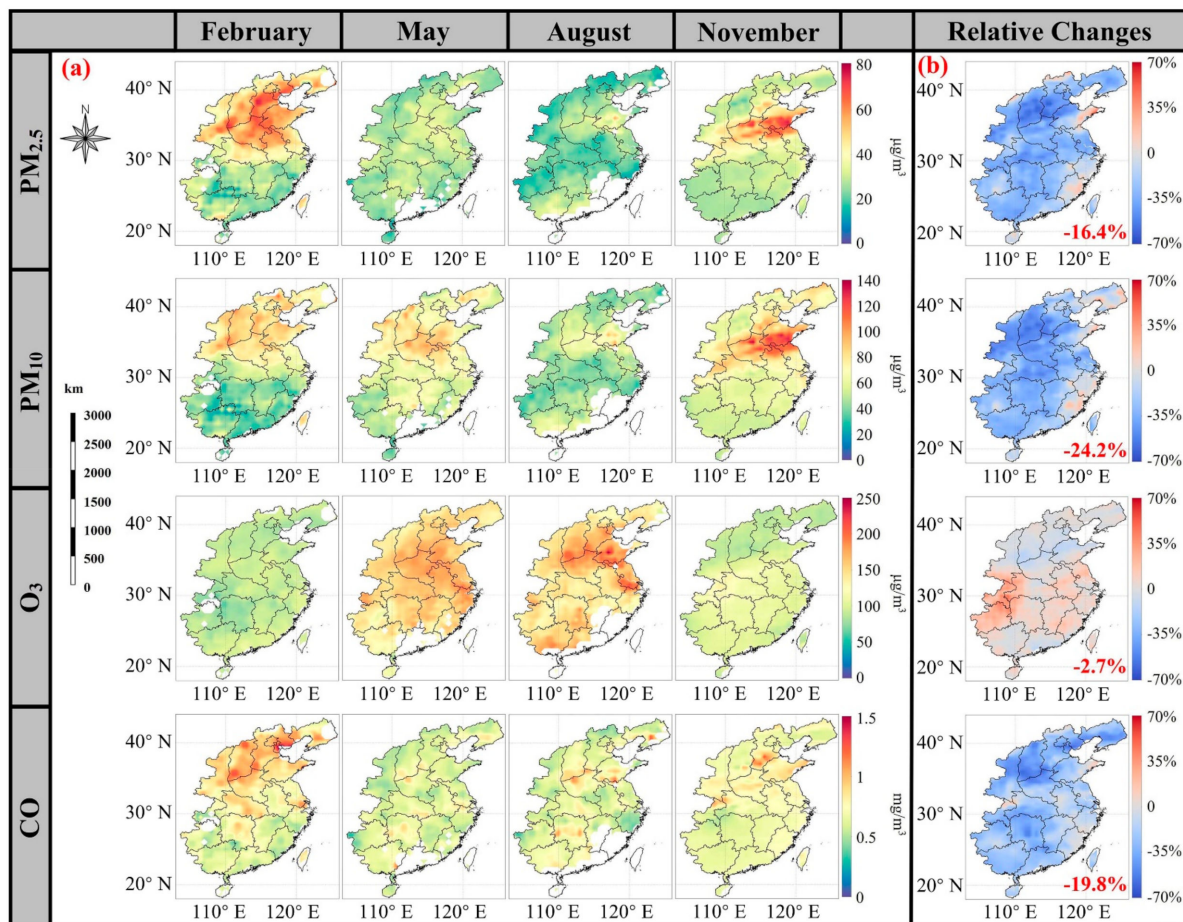


Figure 6. Spatial distributions of model-predicted $PM_{2.5}$, PM_{10} , O_3 , and CO concentrations in February, May, August, and November 2020 and their relative annual rates of change. (a) Spatial distributions of $PM_{2.5}$, PM_{10} , O_3 , and CO, respectively; (b) Relative annual average changes in $PM_{2.5}$, PM_{10} , O_3 , and CO concentrations, respectively. White area indicates no data.

Figure 7 presents the monthly spatial distributions of RF-model predicted $PM_{2.5}$, PM_{10} , O_3 , and CO concentration averaged from 2018 to 2019 in central and eastern China. Compared with the model-predicted concentrations shown in Figure 7a,b,d), the $PM_{2.5}$, PM_{10} , and CO concentrations decreased markedly (65.24%, 58.39%, and 48.12%, respectively) in the North China Plain (NCP) during the Chinese pandemic lockdown. The significant reduction in $PM_{2.5}$ was linked to the sharp decline in human industrial activity (Bao et al., 2020). The $PM_{2.5}$ and PM_{10} concentrations both decreased by ~25–50% in 2020 in the YRD.

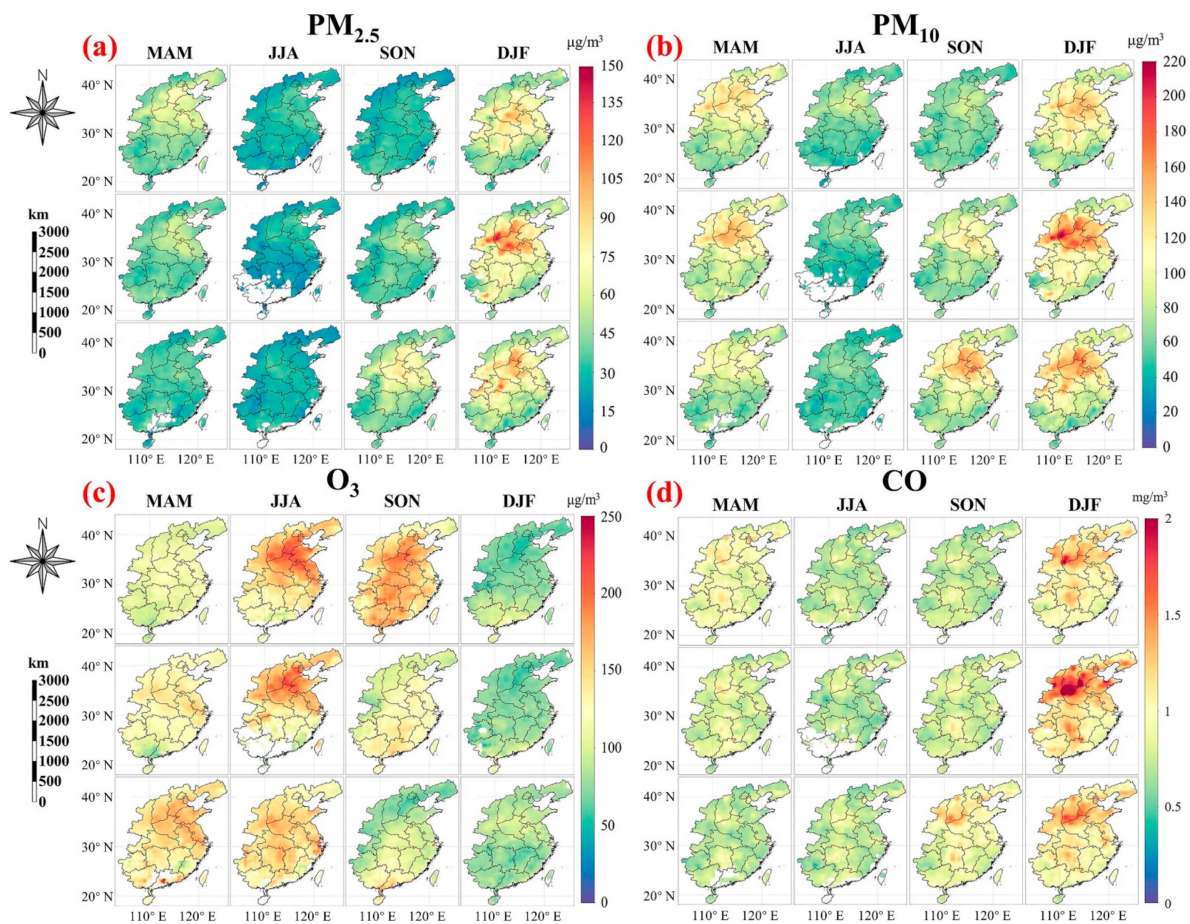


Figure 7. Seasonal spatial distributions of model-predicted $PM_{2.5}$, PM_{10} , O_3 , and CO concentration averaged from 2018 to 2019 over the central and eastern China. (a) $PM_{2.5}$; (b) PM_{10} ; (c) O_3 ; (d) CO. White area indicates no data.

Figure 8 shows the monthly spatial distributions of model-predicted $PM_{2.5}$, PM_{10} , O_3 , and CO concentration in 2020 over the central and eastern China. Interestingly, although the O_3 concentration increased during COVID-19 lockdown, its rate of change was -2.7% in 2020, which may be due to the relatively sharp decline (-22.5%) in summer and autumn compared with the model-predicted concentrations shown in Figures 7c and 8c. The increase in O_3 concentration may be due to the higher temperature ($\sim 1.8^\circ\text{C}$ relative to the averages in 2018 and 2019) in February 2020 [33]. Conversely, due to the weak aerosol scattering and absorption effects caused by the sharp decrease in $PM_{2.5}$ and PM_{10} , higher solar radiation intensity may have led to the increase in O_3 [5]. Notably, the changes in air pollutants are consistent with the spatial distributions expected for the O_3 concentration due to the similar R and RFI results of the other three air pollutants in Figures 2 and 4. Spatially, in the NCP, GBA, and Liaotung Peninsula regions, the O_3 concentration was high but showed a decreasing tendency, whereas in central China, especially Chongqing and Guizhou, the concentration was relatively low but showed an increasing tendency ($\sim 20\text{--}40\%$). In contrast, the level of $PM_{2.5}$ decreased by 32.56% , on average in the above regions. According to previous studies, the O_3 - $PM_{2.5}$ relationship (O_3 is produced, while $PM_{2.5}$ scavenges hydroperoxyl (HO_2) and nitric oxide (NO_x) radicals) may be one of the main reasons for the serious increase in O_3 pollution in these regions [6].

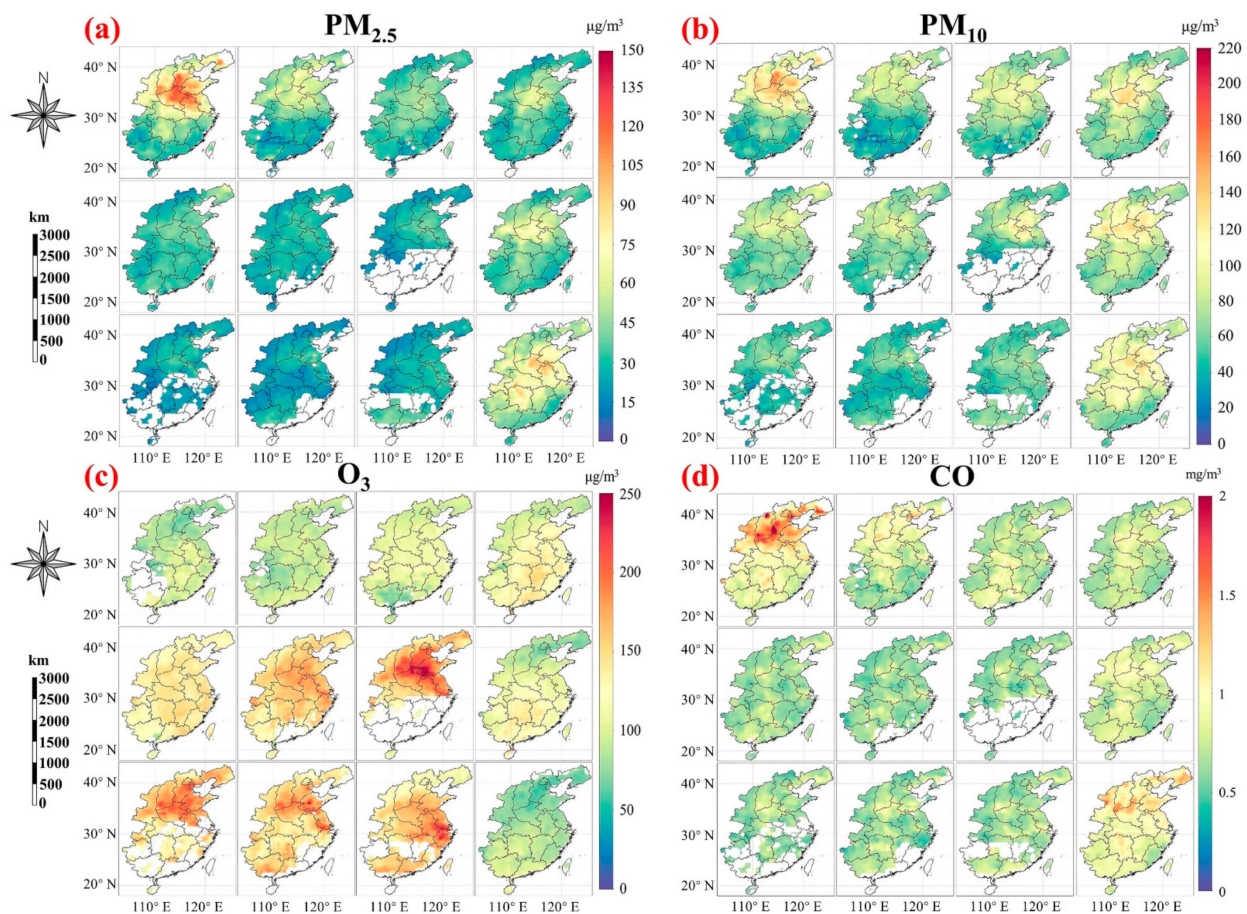


Figure 8. Monthly spatial distributions of model-predicted $\text{PM}_{2.5}$, PM_{10} , O_3 , and CO concentration in 2020 over the central and eastern China. (a) $\text{PM}_{2.5}$; (b) PM_{10} ; (c) O_3 ; (d) CO. White area indicates no data.

Comparing Figures 3b and 7a, we can see that $\text{PM}_{2.5}$ increases more dramatically in low-concentration areas, with PM_{10} and CO showing similar behavior. Specifically, the increases in air pollutants (except for O_3) were obvious (~15–55%, on average, in 2020) in the eastern Shandong Peninsula and southeastern China. However, the changes in O_3 were reversed (i.e., decreased by ~5–20%) compared to the changes in the other three pollutants in these areas, which may be explained by the O_3 - $\text{PM}_{2.5}$ inverse relationship [6]. Although the average rate of change for CO was similar to that of $\text{PM}_{2.5}$ and PM_{10} in spatial distribution, the concentration distribution was not consistent, especially in spring and autumn (Figures 7d and 8d). This may be because the concentration of CO was less influenced by AOD (R is 0.23, and RFI is 0.14) compared to regional vehicle exhaust and industrial waste gas [34]. Therefore, reducing emissions and controlling anthropogenic activities are effective at alleviating air pollution in central and eastern China.

3.3. Seasonal Changes in Air Pollutants in 2020 Compared to 2018 and 2019

The predicted means and standard deviations of the $\text{PM}_{2.5}$, PM_{10} , O_3 , and CO concentrations are presented in Figure 9. The $\text{PM}_{2.5}$, PM_{10} , and CO concentrations all reach the minimum values in summer 2018–2020, but O_3 reaches the maximum value in summer 2018–2020. The rapid changes in PM_{10} in 2018–2019 occurred in April, but occurred in February for 2019–2020, which may be due to differences in policy implementation. Additionally, the changes in PM_{10} (−25.8%) in January 2019–2020 were stronger than that of $\text{PM}_{2.5}$ (−13.3%), suggesting that PM_{10} may be more heavily influenced by policy changes than $\text{PM}_{2.5}$.

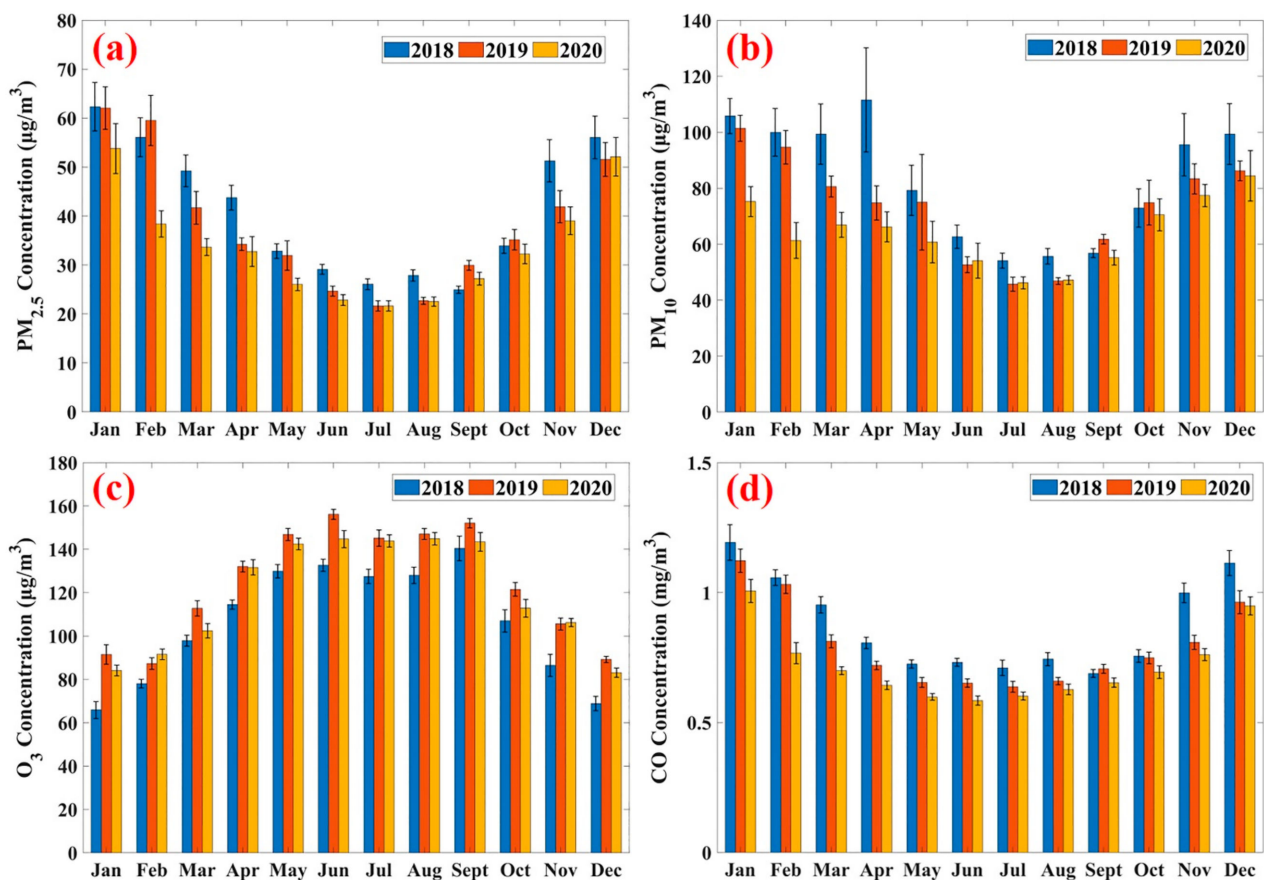


Figure 9. Mean concentrations changes of PM_{2.5}, PM₁₀, O₃, and CO based on geographical RF model from 2018 to 2020. (a) PM_{2.5}, (b) PM₁₀, (c) O₃, and (d) CO.

Figure 10 shows the daily changes in PM_{2.5}, PM₁₀, O₃, and CO concentrations and their linear trends from 2018 to 2020. Results showed that PM_{2.5}, PM₁₀, and CO declined rapidly in February 2020 (44.1%, 43.2%, and 35.9%, respectively) relative to average levels in 2018 and 2019, and their attenuation effects lasted until May (Figures 4 and 10). Similar results have been reported in previous research [13,35]. The changes in PM_{2.5} and PM₁₀ in the summer of 2020 were not significant, which may be due to the resumption of production [15].

However, the trends of the four air pollutants all reversed in September and October 2020 (decreasing) relative to those in 2018–2019 (increasing) (Figures 4 and 10), which may be linked to the joint attenuation effects of the CAAP and COVID-19 lockdown. Similar seasonal changes in PM_{2.5}, PM₁₀, O₃, and CO in 2020 were also predicted from the models, as shown in Figures 7 and 8. Although the declines in O₃ concentration were weaker than those of the other three air pollutants, O₃ still presented a reversing trend (i.e., rates of change in 2018–2019 and 2019–2020 were 0.0349 and -0.0337 µg/m³/day, respectively). Moreover, the attenuation of air pollutants after lockdown accounted for a large proportion of the annual reduction in 2020.

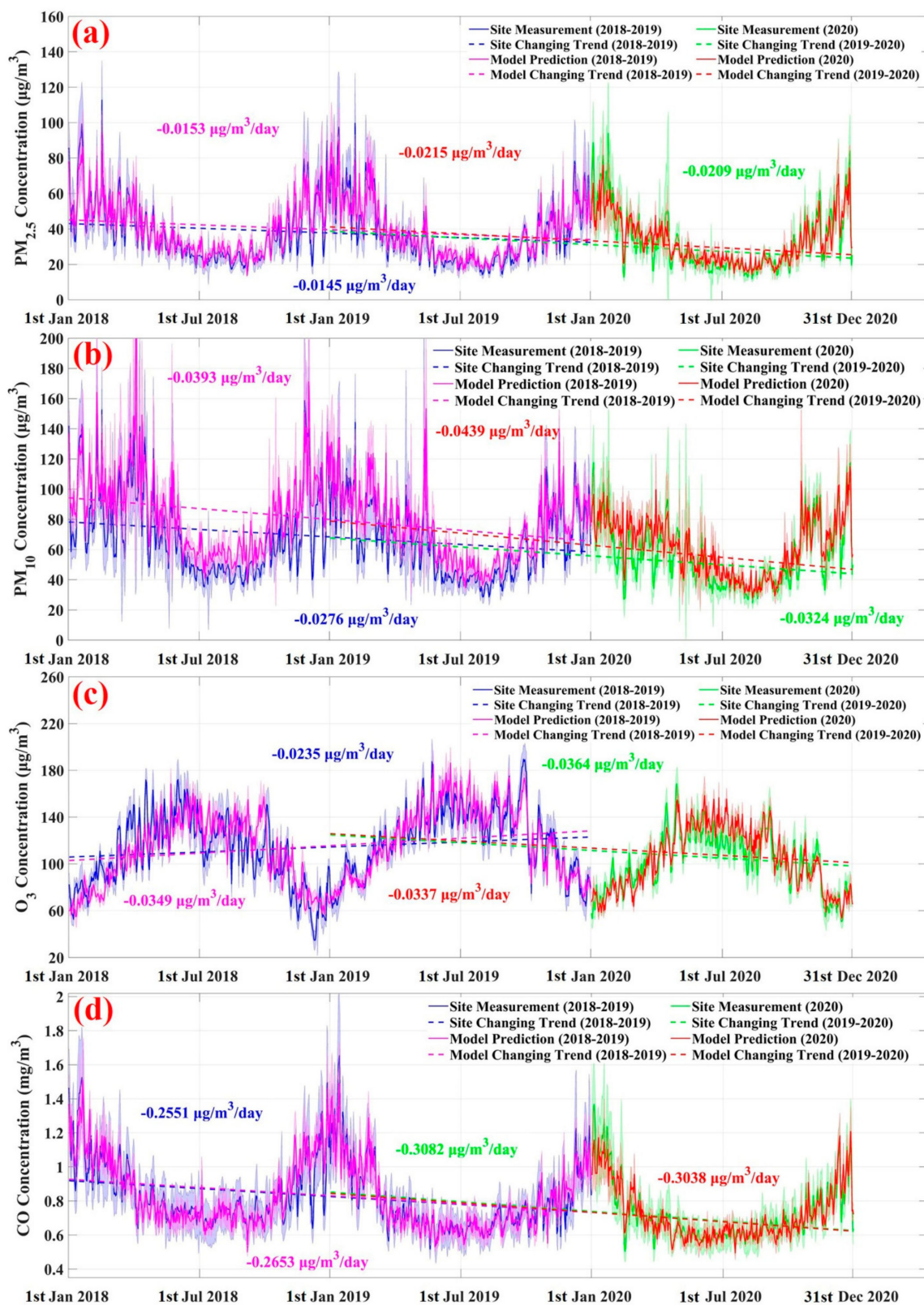


Figure 10. The three-year time series changes of daily PM_{2.5}, PM₁₀, O₃, and CO concentration based on site measurement and model prediction from 1 January 2018 to 31 December 2020 over the Central and Eastern China. (a) The changes for PM_{2.5}; (b) PM₁₀; (c) O₃; (d) CO.

Figure 10 and Table 1 show that the ground-based observations of changes in air pollutants were relatively consistent with the model predictions, but the rates of changes showed slight differences due to different spatial coverage. However, the model predictions may slightly underestimate the concentrations under extreme weather conditions [32]. Although the reduction ratio of PM₁₀ was larger than that of PM_{2.5} in 2019–2020, PM_{2.5} was more strongly influenced by COVID-19 lockdown than PM₁₀. As shown in Figure 4, PM_{2.5} was the only air pollutant to show a sharply reversing trend in February 2020. Moreover, as shown in Figure 10, the change in O₃ concentration was inversely proportional to that of CO, which may be due to their opposite correlation with temperature (0.42 for O₃, −0.38 for CO). Likewise, the similar correlations between PM_{2.5} and PM₁₀ (Figure 2) with input variables may explain their consistent trends in 2018–2020. The three-year time series trends in the concentrations of the air pollutants are consistent with previous studies from 2014 to 2016 [2].

Table 1. The rates of changes of daily PM_{2.5}, PM₁₀, O₃, and CO concentration based on site measurement and model prediction from 1 January 2018 to 31 December 2020 over Central and Eastern China.

Air Pollutant Type	Rate of Change (2018–2019) Unit: $\mu\text{g}/\text{m}^3/\text{day}$		Rate of Change (2019–2020) Unit: $\mu\text{g}/\text{m}^3/\text{day}$	
	Site	Model	Site	Model
	Measurement	Prediction	Measurement	Prediction
PM _{2.5}	−0.0145	−0.0153	−0.0209	−0.0215
PM ₁₀	−0.0276	−0.0393	−0.0324	−0.0439
O ₃	0.0235	0.0349	−0.0364	−0.0337
CO	−0.2551	−0.2653	−0.3082	−0.3038

4. Conclusions

We used ground-based observations, re-analysis, and satellite remote sensing data based on ML to analyze the annual and seasonal changes in primary air pollutants over central and eastern China and explore the joint impact of COVID-19 lockdowns and the CAAP on ambient pollution. The RMSE for the PM_{2.5}, PM₁₀, O₃, and CO validation dataset were 9.027 $\mu\text{g}/\text{m}^3$, 20.312 $\mu\text{g}/\text{m}^3$, 10.436 $\mu\text{g}/\text{m}^3$, and 0.097 mg/m^3 , respectively. The differences between the predicted and observed concentrations of PM_{2.5}, PM₁₀, O₃, and CO were statistically acceptable, and the geographical RF model showed good performance ($R^2 = 0.883$, RMSE within permissible range) for the four pollutants, indicating that the selected variables were able to explain the changes in the pollutants.

Relative to their concentrations in 2018–2019, the concentrations of PM_{2.5}, PM₁₀, and CO in February 2020 decreased by 44.1%, 43.2%, and 35.9%, respectively. These reductions were influenced by the COVID-19 lockdown and lasted until May 2020. The overall increasing trend in the concentration of O₃ was arrested and reversed in 2020. Interestingly, the 2019–2020 trends of the four pollutants all reversed in September and October 2020 relative to the levels observed in 2018–2019, which may be due to the joint effects of the CAAP and COVID-19 lockdown.

Spatially, the concentrations of PM_{2.5}, PM₁₀, and CO showed decreasing trends in almost all regions of central and eastern China, and decreased by 16.4%, 24.2%, and 19.8%, respectively, in 2020 relative to the average levels in 2018 and 2019. The average rate of O₃ change was −2.7% in 2020. Although areas with high O₃ concentration (NCP, GBA, and Liaotung Peninsula) showed declining trends, the government need still needs to pay attention to uncontaminated areas due to the overall increasing trends (~20–40%). The effect of COVID-19 lockdowns on PM_{2.5} was stronger than that on PM₁₀, but the annual average rate of PM₁₀ change influenced by policy was larger. Overall, under the combined influence of the CAAP and COVID-19 lockdowns, the ambient air quality improved, but preparations are still required to prevent future haze events.

Supplementary Materials: The following are available online at <https://www.mdpi.com/article/10.3390/rs13132525/s1>: Figure S1. The detailed structures of RF algorithm for the PM_{2.5}. As the maximum depth of RF algorithm is 15, only the first four levels of decision trees are displayed; Figure S2. The detailed structures of RF algorithm for the PM₁₀. As the maximum depth of RF algorithm is 15, only the first four levels of decision trees are displayed; Figure S3. The detailed structures of RF algorithm for the O₃. As the maximum depth of RF algorithm is 15, only the first four levels of decision trees are displayed; Figure S4. The detailed structures of RF algorithm for the CO. As the maximum depth of RF algorithm is 15, only the first four levels of decision trees are displayed.

Author Contributions: Conceptualization, Z.S., X.H., Y.B.; methodology, Z.S., X.H., Y.B.; data analyses and field investigation, Z.S., X.H., Y.B., D.W.; visualization, D.W., T.L.; data interpretation, Z.S., D.W.; writing—original draft, Z.S., X.H., Y.B.; writing—review and editing, X.H., Y.B., T.L.; supervision, X.H., Y.B.; project administration, X.H. and Y.B. All authors have read and agreed to the published version of the manuscript.

Funding: This research was funded by the National Key Research and Development Program of China (Grant #2017YFA0603003), the National Natural Science Foundation of China (Grants #41825014), the Key Special Project for Introduced Talents Team of Southern Marine Science and Engineering Guangdong Laboratory (Guangzhou) (GML2019ZD0602), the Zhejiang Provincial Natural Science Foundation of China (2017R52001), and the Zhejiang Talent Program (LR18D060001).

Institutional Review Board Statement: Not applicable.

Informed Consent Statement: Not applicable.

Data Availability Statement: The ground-based observational data of air pollutant concentrations were provided by the CNEMC (<http://www.cnemc.cn/en/>, accessed on 10 May 2021). VIIRS data were obtained from NASA LAADS DAAC (<https://ladsweb.modaps.eosdis.nasa.gov/search/>, accessed on 10 May 2021). The ERA5 re-analysis dataset was downloaded from <https://cds.climate.copernicus.eu/#!/home> (accessed on 10 May 2021).

Acknowledgments: We gratefully acknowledge NASA LAADS DAAC for providing the VIIRS data, and the European Centre for Medium-Range Weather Forecast (ECMWF) for providing the ERA5 data used in this study. We thank the China National Environmental Monitoring Center (CNEMC) for providing air pollutant concentrations. We thank SOED/SIO/MNR satellite ground station, satellite data processing & sharing center, and marine satellite data online analysis platform (SatCO2) for their help with data collection and processing.

Conflicts of Interest: The authors declare no conflict of interest.

References

1. Li, R.; Mao, H.; Wu, L.; He, J.; Ren, P.; Li, X. The evaluation of emission control to PM concentration during Beijing APEC in 2014. *Atmos. Pollut. Res.* **2016**, *7*, 363–369. [[CrossRef](#)]
2. Song, C.; Wu, L.; Xie, Y.; He, J.; Chen, X.; Wang, T.; Lin, Y.; Jin, T.; Wang, A.; Liu, Y.; et al. Air pollution in China: Status and spatiotemporal variations. *Environ. Pollut.* **2017**, *227*, 334–347. [[CrossRef](#)] [[PubMed](#)]
3. Chinese State Council. Action Plan on Air Pollution Prevention and Control 2013. Available online: http://www.gov.cn/zwggk/2013-09/12/content_2486773.htm (accessed on 10 May 2021).
4. Zhang, M.; Liu, X.; Sun, X.; Wang, W. The influence of multiple environmental regulations on haze pollution: Evidence from China. *Atmos. Pollut. Res.* **2020**, *11*, 170–179. [[CrossRef](#)]
5. Zhao, S.; Yin, D.; Yu, Y.; Kang, S.; Qin, D.; Dong, L. PM_{2.5} and O₃ pollution during 2015–2019 over 367 Chinese cities: Spatiotemporal variations, meteorological and topographical impacts. *Environ. Pollut.* **2020**, *264*, 114694. [[CrossRef](#)] [[PubMed](#)]
6. Li, K.; Jacob, D.J.; Liao, H.; Zhu, J.; Shah, V.; Shen, L.; Bates, K.H.; Zhang, Q.; Zhai, S. A two-pollutant strategy for improving ozone and particulate air quality in China. *Nat. Geosci.* **2019**, *12*, 906–910. [[CrossRef](#)]
7. Chen, L.; Zhu, J.; Liao, H.; Yang, Y.; Yue, X. Meteorological influences on PM_{2.5} and O₃ trends and associated health burden since China's clean air actions. *Sci. Total Environ.* **2020**, *744*, 140837. [[CrossRef](#)] [[PubMed](#)]
8. Chinese State Council. Three-Year Action Plan on Defending the Blue Sky. 2018. Available online: http://www.gov.cn/zhengce/content/2018-07/03/content_5303158.htm (accessed on 10 May 2021). (In Chinese)
9. Bauwens, M.; Compennolle, S.; Stavrakou, T.; Müller, J.; van Gent, J.; Eskes, H.; Levelt, P.F.; van der A., R.; Veefkind, J.P.; Vlietinck, J.; et al. Impact of coronavirus outbreak on NO₂ pollution assessed using TROPOMI and OMI observations. *Geophys. Res. Lett.* **2020**, *47*, e2020GL087978. [[CrossRef](#)] [[PubMed](#)]
10. Ding, J.; van der A., R.J.; Eskes, H.J.; Mijling, B.; Stavrakou, T.; van Geffen, J.H.G.M.; Veefkind, J.P. NO_x emissions reduction and rebound in China due to the COVID-19 crisis. *Geophys. Res. Lett.* **2020**, *47*. [[CrossRef](#)]

11. Griffith, S.M.; Huang, W.-S.; Lin, C.-C.; Chen, Y.-C.; Chang, K.-E.; Lin, T.-H.; Wang, S.-H.; Lin, N.-H. Long-range air pollution transport in East Asia during the first week of the COVID-19 lockdown in China. *Sci. Total Environ.* **2020**, *741*, 140214. [[CrossRef](#)]
12. Huang, X.; Ding, A.; Gao, J.; Zheng, B.; Zhou, D.; Qi, X.; Tang, R.; Wang, J.; Ren, C.; Nie, W.; et al. Enhanced secondary pollution offset reduction of primary emissions during COVID-19 lockdown in China. *Natl. Sci. Rev.* **2020**, *8*. [[CrossRef](#)]
13. Liu, L.; Zhang, J.; Du, R.; Teng, X.; Hu, R.; Yuan, Q.; Tang, S.; Ren, C.; Huang, X.; Xu, L.; et al. Chemistry of Atmospheric Fine Particles During the COVID-19 pandemic in a megacity of eastern China. *Geophys. Res. Lett.* **2020**, *48*. [[CrossRef](#)]
14. Bao, R.; Zhang, A. Does lockdown reduce air pollution? Evidence from 44 cities in northern China. *Sci. Total Environ.* **2020**, *731*, 139052. [[CrossRef](#)]
15. Sun, Y.; Lei, L.; Zhou, W.; Chen, C.; He, Y.; Sun, J.; Li, Z.; Xu, W.; Wang, Q.; Ji, D.; et al. A chemical cocktail during the COVID-19 outbreak in Beijing, China: Insights from six-year aerosol particle composition measurements during the Chinese New Year holiday. *Sci. Total Environ.* **2020**, *742*, 140739. [[CrossRef](#)]
16. Nichol, J.; Bilal, M.; Ali, A.; Qiu, Z. Air pollution scenario over China during COVID-19. *Remote Sens.* **2020**, *12*, 2100. [[CrossRef](#)]
17. Li, L.; Liu, X.; Ge, J.; Chu, X.; Wang, J. Regional differences in spatial spillover and hysteresis effects: A theoretical and empirical study of environmental regulations on haze pollution in China. *J. Clean. Prod.* **2019**, *230*, 1096–1110. [[CrossRef](#)]
18. Chang, Y.; Huang, R.; Ge, X.; Huang, X.; Hu, J.; Duan, Y.; Zou, Z.; Liu, X.; Lehmann, M.F. Puzzling haze events in China during the coronavirus (COVID-19) shutdown. *Geophys. Res. Lett.* **2020**, *47*, e2020GL088533. [[CrossRef](#)]
19. Hites, R.A.; Lehman, D.C.; Salamova, A.; Venier, M. Temporal environmental hysteresis: A definition and implications for polybrominated diphenyl ethers. *Sci. Total Environ.* **2021**, *753*, 141849. [[CrossRef](#)]
20. Yin, S.; Wang, X.; Xiao, Y.; Tani, H.; Zhong, G.; Sun, Z. Study on spatial distribution of crop residue burning and PM_{2.5} change in China. *Environ. Pollut.* **2017**, *220*, 204–221. [[CrossRef](#)]
21. Lai, I.-C.; Lee, C.-L.; Huang, H.-C. A new conceptual model for quantifying transboundary contribution of atmospheric pollutants in the East Asian Pacific rim region. *Environ. Int.* **2016**, *88*, 160–168. [[CrossRef](#)]
22. Lee, S.; Ho, C.-H.; Lee, Y.G.; Choi, H.-J.; Song, C.-K. Influence of transboundary air pollutants from China on the high-PM₁₀ episode in Seoul, Korea for the period October 16–20, 2008. *Atmos. Environ.* **2013**, *77*, 430–439. [[CrossRef](#)]
23. Lary, D.; Alavi, A.H.; Gandomi, A.; Walker, A.L. Machine learning in geosciences and remote sensing. *Geosci. Front.* **2016**, *7*, 3–10. [[CrossRef](#)]
24. Liu, R.Y.; Ma, Z.W.; Liu, Y.; Shao, Y.C.; Zhao, W.; Bi, J. Spatiotemporal distributions of surface ozone levels in China from 2005 to 2017: A machine learning approach. *Environ. Int.* **2020**, *142*, 105823. [[CrossRef](#)] [[PubMed](#)]
25. Wei, J.; Huang, W.; Li, Z.; Xue, W.; Peng, Y.; Sun, L.; Cribb, M. Estimating 1-km-resolution PM_{2.5} concentrations across China using the space-time random forest approach. *Remote Sens. Environ.* **2019**, *231*, 111221. [[CrossRef](#)]
26. Zhan, Y.; Luo, Y.; Deng, X.; Chen, H.; Grieneisen, M.L.; Shen, X.; Zhu, L.; Zhang, M. Spatiotemporal prediction of continuous daily PM_{2.5} concentrations across China using a spatially explicit machine learning algorithm. *Atmos. Environ.* **2017**, *155*, 129–139. [[CrossRef](#)]
27. National Bureau of Statistics of China. China Statistical Yearbook 2019. 2019. Available online: <http://www.stats.gov.cn/tjsj/ndsj/2019/indexeh.htm> (accessed on 10 May 2021).
28. Chen, G.; Li, S.; Knibbs, L.; Hamm, N.; Cao, W.; Li, T.; Guo, J.; Ren, H.; Abramson, M.J.; Guo, Y. A machine learning method to estimate PM_{2.5} concentrations across China with remote sensing, meteorological and land use information. *Sci. Total Environ.* **2018**, *636*, 52–60. [[CrossRef](#)]
29. Chen, G.; Wang, Y.; Li, S.; Cao, W.; Ren, H.; Knibbs, L.; Abramson, M.J.; Guo, Y. Spatiotemporal patterns of PM₁₀ concentrations over China during 2005–2016: A satellite-based estimation using the random forests approach. *Environ. Pollut.* **2018**, *242*, 605–613. [[CrossRef](#)]
30. Jones, Z.M.; Linder, F.J. edarf: Exploratory data analysis using random forests. *J. Open Source Softw.* **2016**, *1*, 92. [[CrossRef](#)]
31. Vu, T.V.; Shi, Z.; Cheng, J.; Zhang, Q.; He, K.; Wang, S.; Harrison, R.M. Assessing the impact of clean air action on air quality trends in Beijing using a machine learning technique. *Atmos. Chem. Phys.* **2019**, *19*, 11303–11314. [[CrossRef](#)]
32. Liu, J.; Weng, F.; Li, Z. Satellite-based PM_{2.5} estimation directly from reflectance at the top of the atmosphere using a machine learning algorithm. *Atmos. Environ.* **2019**, *208*, 113–122. [[CrossRef](#)]
33. Wang, T.; Xue, L.; Brimblecombe, P.; Lam, Y.F.; Li, L.; Zhang, L. Ozone pollution in China: A review of concentrations, meteorological influences, chemical precursors, and effects. *Sci. Total Environ.* **2017**, *575*, 1582–1596. [[CrossRef](#)]
34. Fan, H.; Zhao, C.; Ma, Z.; Yang, Y. Atmospheric inverse estimates of CO emissions from Zhengzhou, China. *Environ. Pollut.* **2020**, *267*, 115164. [[CrossRef](#)]
35. Su, T.; Li, Z.; Zheng, Y.; Luan, Q.; Guo, J. Abnormally shallow boundary layer associated with severe air pollution during the COVID-19 lockdown in China. *Geophys. Res. Lett.* **2020**, *47*, e2020GL090041. [[CrossRef](#)]